

INFERRING THE PALEO-LONGITUDE DIRECTLY FROM THE PALEO-GEOMAGNETIC DATA

RONG QIANG WEI

ABSTRACT. Knowledge of the ancient geology and tectonics of the Earth owes much to paleo-magnetism. However, it is thought that paleo-magnetism has the incapability in providing paleo-longitude. To obtain this important location parameter many other indirect methods have been developed based on different assumptions. Here we present a direct method to derive the paleo-longitude from the usual paleo-magnetic measurements. This method takes into account the contributions to the Earth's magnetic potential from additional dipoles with their axes in the equatorial plane, which were omitted by the traditional paleo-magnetism. Two explicit formulae for inferring the longitude are obtained. It is shown in synthetic experiments that longitudes can be perfectly derived through these formulae, from the measured components of magnetic field (B_x, B_y, B_z), or declination (D) and inclination(I). The errors are mainly from B_x, B_z or I . Thus these two explicit formulae can be used in paleo-magnetism as an alternative approach to estimate the paleo-longitude. By this direct approach, we infer the synthetic paleo-longitudes for the reference points in the continents of North America, Eurasia, and India for the last 200 Ma and a reference paleo-longitude for Indo-Asia collision based on paleo-magnetic data. The synthetic trajectories of these reference points, which determined by synthetic paleo-longitudes and paleo-latitudes, show the movements of these three continents had their own respective properties. All of them included different both translation and rotation in four phases. The paleo-longitude for India-Asia collision was at $132.6_{-14.7}^{+27.2}$ ° E.

Keywords: paleo-longitude; paleo-magnetism; paleo-magnetic data; plate tectonic reconstructions

1. INTRODUCTION

Obtaining quantitatively the paleo-position of continents is essential to the plate tectonic reconstructions. The paleo-position of the continents includes basically the paleo-longitude λ and the paleo-latitude ϕ in the past. The ϕ of the continents can be traditionally inferred from the paleo-magnetic data of inclination I , ie., $\tan \phi = \frac{1}{2} \tan I$ (eg., Turcotte and Schubert, 2014). This inferring is based on the assumption that the Earths paleo-magnetic field at some geo-time (or geo-time-averaged field) can be approximated as a dipole field. Such a dipole field can be modeled through a Gaussian spherical harmonic expansion with $n = 1$ and the Gauss coefficient g_1^1 and h_1^1 equal to zero (see details in the section 2). In this case, the paleo-magnetic field is axis symmetric and can not provide any information on the paleo-longitude.

To obtain the paleo-longitude of the continents, many methods other than paleo-magnetism were developed, and different reference frames were constructed. Some authors established

the hot spots absolute plate motion reference frame (e.g., Müller et al., 1993; O' Neill et al., 2005; Torsvik et al., 2008a; Doubrovine et al., 2012), for the motion of the lithospheric plates may be reflected by the track geometry of the hot spots (Morgan, 1971). A global hybrid reference frame, by correlating large igneous provinces and deep mantle heterogeneities at the core-mantle boundary, was established by Torsvik et al. (2008b). This reference frame assumed zero longitudinal motion of Africa before 100 Ma. By modeling of plume motions, these reference frames provided compatible reconstructions of plates with geologic and geophysical data (e.g., Doubrovine et al., 2012). Besides, van der Meer et al. (2010) linked the lower mantle slab remnants with the global orogenic belts reconstructions, and established a sinking slab remnant reference frame. This reference frame assumed a vertical slab sinking at an average rate of 12 ± 3 mm/yr.

On the other hand, researchers attempted to estimate paleo-longitude from the data associated with paleo-magnetism, especially the data of polar wander path (PWP). For example, Mitchell et al. (2012) traced the moving trajectory of supercontinents centers in the deep geologic history and presented a true PWP derived reference frame, in which they assumed the stable geoid highs. Wu and Kravchinsky (2014) and Wu et al. (2015) presented a synthesized method to derive paleo-longitude by geometrically parametrizing apparent PWP. The method restores the absolute motion history for the reference geometries from the Euler parameters extracted from the apparent PWPs. In this method, a paleo-colatitude correction to the reconstructions was introduced in order to keep the restored paleo-latitudes compatible with the paleo-magnetic prediction.

Although based on different assumptions, these work above are helpful to estimate the paleo-position of the continents, and to understand how the fragments of the outer shell of the Earth have moved relative to a reference system over geological timescales. Here we present another alternative method to infer the paleo-longitudes from the usual paleo-magnetic measurements. The related theory will be given in section 2. Because the inferring the paleo-longitude based on this theory is a nonlinear problem, we present a simple approach to solve it. Then we test this method with synthesized data, and discuss the error from different sources in the section 3. In the section 4 we provide synthetic paleo-longitude for the continents of North America, Eurasia, and India for the last 200 Ma based on the synthetic data; And estimate a reference paleo-longitude for Indo-Asia collision. Finally we give a short discussion in the section 5 and draw some conclusions in the section 6.

2. THEORY AND METHODOLOGY

2.1. Theory. We start from the well-known Gauss's spherical expression for the potential of the geomagnetic field,

$$(1) \quad V = a \sum_{n=1}^{\infty} \sum_{m=0}^n \left(\frac{a}{r}\right)^{n+1} P_n^m(\theta) (g_n^m \cos m\lambda + h_n^m \sin m\lambda)$$

where a is the Earth's radius, $P_n^m(\theta)$ Schmidt polynomials which are related to the associated Legendre polynomials, g_n^m and h_n^m Gauss coefficients of order n and degree m , r the distance from the Earth's center, θ colatitude and λ longitude.

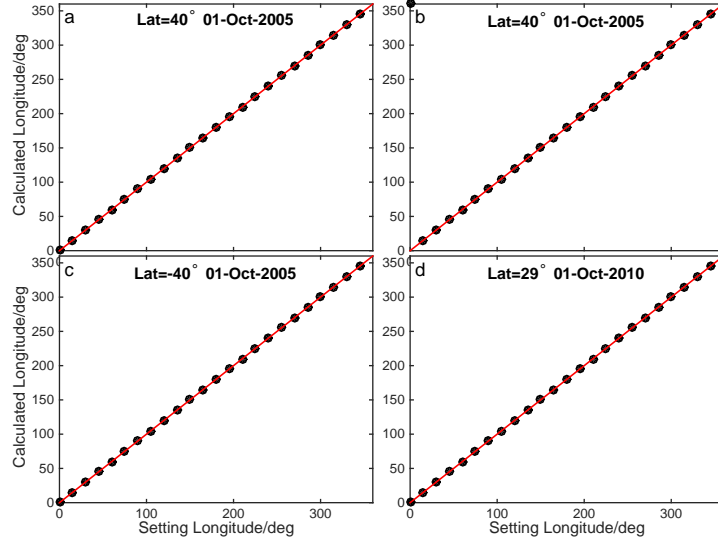


Fig. 1: Longitudes derived from Equation (7) and (9) vs. the setting longitudes. (a) Longitudes are derived with Equation (7); (b), (c), (d), Longitudes are from Equation (9). B_x, B_y, B_z, D, I are from International Geomagnetic Reference Field (IGRF) model.

Generally $V_1 = V|_{n=1}$ is taken as the potential of the centered dipole field, which is a first order approximation but the most important part of the geomagnetic field.

$$(2) \quad V_1 = \frac{a^3}{r^2} (g_1^0 \cos \theta + g_1^1 \sin \theta \cos \lambda + h_1^1 \sin \theta \sin \lambda)$$

where the term g_1^0 is the strongest component of the field. It describes a magnetic dipole at the center of the Earth and aligned with the Earth's rotation axis. The terms g_1^1 and h_1^1 are the next strongest parts. They describe contributions to the magnetic potential from additional dipoles with their axes in the equatorial plane.

One can obtain the components of the geomagnetic dipole field B_x, B_y, B_z at the surface as the following,

$$(3) \quad \left\{ \begin{array}{lcl} B_x = -\frac{1}{r} \frac{\partial V}{\partial \theta} |_{r=a} & \approx -\frac{1}{r} \frac{\partial V_1}{\partial \theta} |_{r=a} & = g_1^0 \sin \theta - (g_1^1 \cos \lambda + h_1^1 \sin \lambda) \cos \theta \\ B_y = -\frac{1}{r \sin \theta} \frac{\partial V}{\partial \lambda} |_{r=a} & \approx -\frac{1}{r \sin \theta} \frac{\partial V_1}{\partial \lambda} |_{r=a} & = g_1^1 \sin \lambda - h_1^1 \cos \lambda \\ B_z = -\frac{\partial V}{\partial r} |_{r=a} & \approx -\frac{\partial V_1}{\partial r} |_{r=a} & = 2[g_1^0 \cos \theta + (g_1^1 \cos \lambda + h_1^1 \sin \lambda) \sin \theta] \end{array} \right.$$

From equation (3), the longitude λ can be possibly inferred from the measured B_x , B_y , B_z if g_1^0 , g_1^1 and h_1^1 are known. However, g_1^0 , g_1^1 and h_1^1 are generally difficult to be obtained. If let $g_1^1 = h_1^1 = 0$ in equation (3), we can immediately get $B_y = 0$, and

$$(4) \quad \tan I = \frac{B_z}{\sqrt{B_x^2 + B_y^2}} = \frac{B_z}{B_x} = 2 \cot \theta$$

where I is the magnetic inclination. Equation (4) is the foundational equation of the usual paleo-magnetism. It can be seen that only θ (then the latitude) appears.

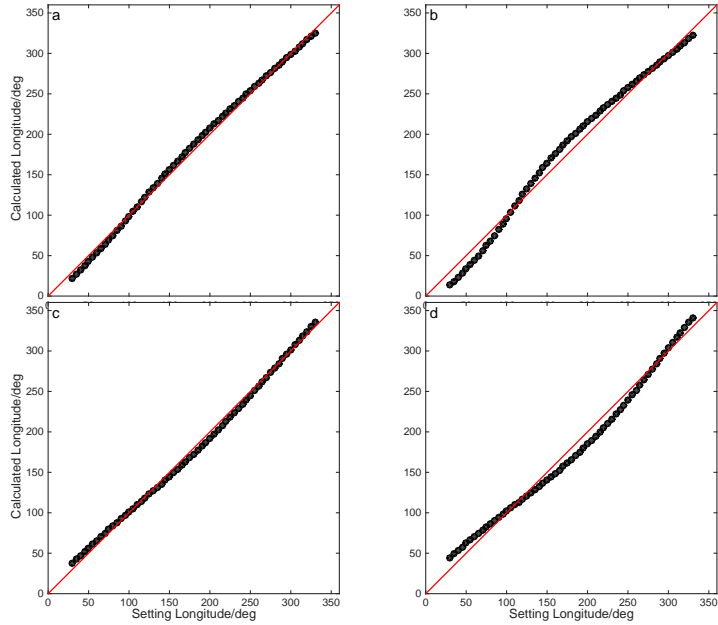


Fig. 2: Longitudes derived from Equation (9) vs. the setting longitudes when B_x is add a perturbation of -5% (a), -10% (b), 5% (c), and 10% (d). B_x, B_y, B_z at the surface and D, I are from IGRF model on Oct. 1, 2005 and at the latitude of 40° N.

Clearly g_1^1 and h_1^1 can not be omitted in equation (3) to infer λ . g_1^1 and h_1^1 will be taken into account in the following approach we adopt. According to the central dipole model (e.g., Hurwitz, 1960; Alldredge and Hurwitz, 1964; Lanza and Meloni, 2006), Equation (3) can be rewritten as,

$$(5) \quad \begin{cases} B_x = K_p [\cos \theta_p \sin \theta - \sin \theta_p \cos \theta \cos(\lambda - \lambda_p)] \\ B_y = K_p \sin \theta_p \sin(\lambda - \lambda_p) \\ B_z = 2K_p [\cos \theta_p \cos \theta + \sin \theta_p \sin \theta \cos(\lambda - \lambda_p)] \end{cases}$$

where $K_p = M_p/a^3$, and M_p is the magnetic moment for the central radial dipole at colatitude θ_p and east longitude λ_p . It is easy to demonstrate that $g_1^0 = K_p \cos \theta_p$, $g_1^1 = K_p \sin \theta_p \cos \lambda_p$, $h_1^1 = K_p \sin \theta_p \sin \lambda_p$, and $B_x^2 + B_y^2 + (B_z/2)^2 = K_p^2$. Therefore, equation (5) is equivalent to equation (3), and g_1^1 and h_1^1 are naturally included in the equation (5).

From equation (5), the longitude λ , even θ , and K_p , can be possibly inferred if B_x , B_y , B_z , θ_p , and λ_p are known, because these quantities can be measured or estimated relatively easily.

2.2. Methodology. It is not easy to infer λ , even θ , and K_p simultaneously from Equation (5), because it is nonlinear. However, if θ can be estimated firstly in other ways, λ (even K_p) can be easily obtained with the known B_x , B_y , B_z , θ_p , and λ_p .

From Equation (5), one can get,

$$(6) \quad \begin{cases} \cos(\lambda - \lambda_p) &= \frac{\cos \theta_p (\sin \theta - \frac{B_x}{0.5B_z} \cos \theta)}{\sin \theta_p (\cos \theta + \frac{B_x}{0.5B_z} \sin \theta)} \\ \sin(\lambda - \lambda_p) &= \frac{B_y}{K_p \sin \theta_p} \\ K_p &= \pm [B_x^2 + B_y^2 + (\frac{B_z}{2})^2]^{\frac{1}{2}} \end{cases}$$

Further, one can infer λ from Equation (6) as the following,

$$(7) \quad \lambda = \lambda_p + \tan^{-1} \left\{ \pm \frac{B_y \sec \theta_p}{[B_x^2 + B_y^2 + (\frac{B_z}{2})^2]^{\frac{1}{2}}} \cdot \frac{\cos \theta + \frac{B_x}{0.5B_z} \sin \theta}{\sin \theta - \frac{B_x}{0.5B_z} \cos \theta} \right\}$$

One can also get λ with the known declination (D) and inclination(I), θ_p , and λ_p , because the following equations hold (e.g., Kono and Tanaka, 1995).

$$(8) \quad \begin{cases} \frac{B_y}{B_x} &= \tan D \\ \frac{B_x}{0.5B_z} &= 2 \cot I \cos D \\ \tan I &= 2 \cot \theta \\ \sin \theta &= \pm \sqrt{\frac{B_x^2 + B_y^2}{B_x^2 + B_y^2 + (B_z/2)^2}} \end{cases}$$

From Equation (7) and (8), one can obtain,

$$(9) \quad \lambda = \lambda_p + \tan^{-1} \left[\pm \frac{\sin D \sec \theta_p}{\sqrt{\frac{\tan^2 I}{4} + 1}} \cdot \frac{\cos \theta + 2 \cos D \cot I \sin \theta}{\sin \theta - 2 \cos D \cot I \cos \theta} \right]$$

Explicit equation (7) and (9) can be used to infer the λ when θ_p , and λ_p are known and B_x , B_y , B_z (or D , I) are measured.

2.3. Case of the Paleomagnetism. In paleo-magnetic study, if the remanent magnetization J_r of the rocks is assumed to be proportional to B as the following (equation (10)), we can also infer the paleo-longitude λ with the similar procedure above, like equation (7) and (9).

$$(10) \quad \begin{aligned} J_{rx} &\approx k \frac{B_x}{\mu_0} = k' B_x \\ J_{ry} &\approx k \frac{B_y}{\mu_0} = k' B_y \\ J_{rz} &\approx k \frac{B_z}{\mu_0} = k' B_z \end{aligned}$$

where μ_0 is permeability constant ($= 4\pi \times 10^{-7} \text{NA}^{-2}$), k the proportionality constant.

In this case, if θ is firstly estimated from equation (4), and the site longitude λ , site latitude ϕ , magnetic colatitude θ , and D are known, θ_p ($= \frac{\pi}{2} - \phi_p$) and λ_p can be estimated from the well-known formulae as follows,

$$(11) \quad \begin{cases} \sin \phi_p &= \sin \phi \cos \theta + \cos \phi \sin \theta \cos D \\ \sin(\lambda_p - \lambda) &= \frac{\sin \theta \sin D}{\cos \phi_p} & \text{if } \cos \theta > \sin \phi \sin \phi_p \\ \sin(\pi - \lambda_p + \lambda) &= \frac{\sin \theta \sin D}{\cos \phi_p} & \text{if } \cos \theta < \sin \phi \sin \phi_p \end{cases}$$

Remark. If ϕ_p derived from Equation (11) is negative, it means that the geomagnetic north pole in the northern hemisphere corresponds to a magnetic south pole for the dipole at the Earth's center. Then the fraction in the bracket in Equation (7) and (9) is negative, otherwise, positive.

It should be pointed out that the paleo-longitude λ estimated in this way might have errors because the θ , θ_p and λ_p from equation (11) are rough. We will discuss this with synthetic data in section 3.

3. SYNTHETIC EXPERIMENTS

3.1. Inferring longitude from synthetic data. We test Equation (7) and (9) with a series of synthetic experiments at random co-latitudes θ ($= \frac{\pi}{2} - \phi$). The synthetic data, namely, the components of the Earth's magnetic field at the surface, B_x, B_y, B_z for Equation (7), and D, I for Equation (9), are calculated from International Geomagnetic Reference Field (IGRF) model (International Association of Geomagnetism and Aeronomy, Working Group V-MOD, 2010) when $n = 1$, respectively. The time is also given randomly. The setting longitudes are from 0° to 360° at an interval of 5° . λ_p and θ_p are calculated from Gaussian coefficients g_1^0, g_1^1, h_1^1 with the following equation (12) (eg., Lanza and Meloni, 2006),

$$(12) \quad \begin{cases} \lambda_p &= \tan^{-1}(\frac{h_1^1}{g_1^1}) \\ \theta_p &= \cot^{-1}(\frac{g_1^0}{\sqrt{(g_1^1)^2 + (h_1^1)^2}}) \end{cases}$$

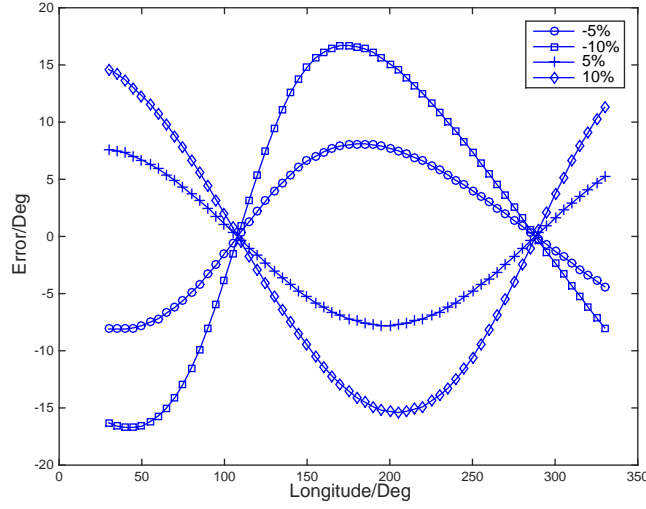


Fig. 3: The errors of longitude caused by a perturbation of B_x when θ , λ_p and θ_p can be obtained or given by other methods accurately. B_x, B_y, B_z at the surface are from IGRF model on Oct. 1, 2005 and at the latitude of 40° N.

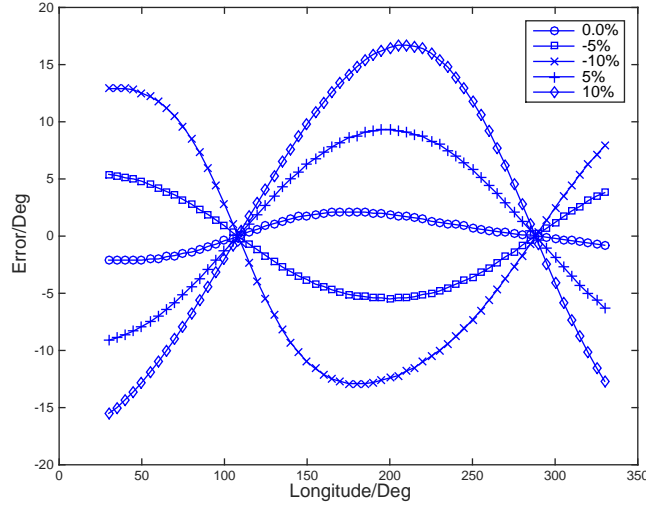


Fig. 4: The errors of longitude caused by a perturbation of B_x when θ , λ_p and θ_p can be derived from B_x, B_y, B_z (or D, I). B_x, B_y, B_z at the surface are from IGRF model on Oct. 1, 2005 and at the latitude of 40° N.

Figure 1 shows the comparison of longitudes derived from Equation (7) and (9) with those setting longitudes for three examples (To see clearly we plot only the longitudes derived at an interval of 15°). It can be seen that the setting longitudes are derived perfectly from both two equations. The numerical results from Equation (7) are equivalent to those from (9). It should be pointed out that λ_p and θ_p can also be derived from equation (11); The results from equation (12) are the same to those from equation (11).

3.2. Error analysis. The quantities, $B_x, B_y, B_z, D, I, \theta, \lambda_p$ and θ_p in Equation (7) and (9), must have errors when they are actually measured or calculated, especially in the paleo-magnetic data. In this subsection we check the errors from these sources, by adding some positive or negative perturbations. Here B_x, B_y, B_z at the surface are from IGRF model on Oct. 1, 2005 and at the latitude of 40° N. For simplicity, the setting longitudes are from 30° E to 330° E, out of which may have nominal great errors. For example, the setting longitude is 0° E, but the derived is 359° E. The true absolute error is 1° but the nominal one is 358° . Furthermore, we adopt the algorithm of the root-mean-square error (RMSE) to calculate a nominal RMSE for errors from these perturbations. This nominal RMSE will be utilized to represent the "mean" error between the setting and the derived longitudes.

Two cases are considered here. The first is that θ, λ_p and θ_p can be obtained or given by other methods accurately, rather than derived from B_x, B_y, B_z (or D, I). We add different perturbations to $B_x, B_y, B_z, D, I, \lambda_p$ and θ_p as shown in Table 1. The corresponding maximum and minimum error, absolute error, and nominal RMSE, respectively, are also shown in Table 1.

We take B_x as an example to illustrate. Figure 2 shows the comparison of the longitudes derived from Equation (7) or (9) with the setting longitudes when B_x is added a perturbation of -5% , -10% , 5% and 10% , respectively. It can be found that the setting longitudes are derived but with small errors at the perturbation of $\pm 5\%$, and larger errors at the perturbation of $\pm 10\%$. Figure 3 shows the errors vary with the setting longitudes. The errors in this case are different with different setting longitudes and fluctuate clearly: For the perturbation of -5% , the maximum negative errors are at two endpoint longitudes; Between them, the error curve is like a parabola going downwards, with a maximum error at about 188° E and the minimum errors at about 108° E and 288° E, respectively. From Table 1 it can be seen that the maximum error is $\pm 8.1^\circ$, the minimum error 0.2° , and the nominal RMSE 5.5° . The error curve for the perturbation of -10% is similar to that of -5% , while those error curves for the positive perturbation have the properties of mirror symmetry with those for the negative perturbations.

From Table 1, it is found that the errors caused by the perturbation of B_x is the largest, then B_z , then λ_p , then I , then D , then B_y , and the last is the θ_p . The simplest errors, which are constant, are from λ_p . This can be inferred from equation (7) and (9).

In the end, we add simultaneously some equal perturbations to $B_x, B_y, B_z, D, I, \lambda_p$ and θ_p . It is found that the maximum negative error is -1.5° , maximum error 8.7° , the minimum absolute error 0.0° , and the nominal RMSE 4.9° for the perturbation of -5% . More details can be seen in Table 1.

Table 1: Errors caused by B_x , B_y , B_z , etc., when θ , λ_p and θ_p can be obtained or given by other methods rather than derived from B_x , B_y , B_z (or D , I).

Variable (Perturbation)	e_{min} (°E)	e_{max} (°E)	$ e _{min}$ (°E)	$ e _{max}$ (°E)	nRMSE (°E)
B_x (-5%)	-8.1	8.1	0.2	8.1	5.5
B_x (-10%)	-16.7	16.7	0.4	16.7	11.4
B_x (5%)	-7.8	7.6	0.3	7.8	5.2
B_x (10%)	-15.4	14.6	0.5	15.4	10.2
B_y (-5%)	-1.4	1.4	0.1	1.4	1.0
B_y (-30%)	-10.0	10.0	0.6	10.0	7.1
B_y (5%)	-1.4	1.4	0.1	1.4	1.0
B_y (30%)	-10.0	10.0	0.4	7.4	5.3
B_z (-5%)	-8.3	7.1	0.2	8.3	5.3
B_z (-10%)	-17.2	15.6	0.3	17.2	10.9
B_z (5%)	-7.5	7.8	0.2	7.8	5.1
B_z (10%)	-15.1	15.3	0.5	15.3	10.2
D (-5%)	-1.6	1.6	0.1	1.6	1.1
D (-20%)	-6.9	6.9	0.3	6.9	4.6
D (5%)	-1.5	1.5	0.1	1.5	1.0
D (20%)	-5.7	5.7	0.3	5.7	3.8
I (-5%)	-6.2	6.2	0.2	6.2	4.2
I (-10%)	-10.2	10.2	0.4	10.2	7.4
I (5%)	-6.5	6.6	0.2	6.6	3.4
I (10%)	-12.4	12.6	0.2	12.6	6.9
λ_p (-5%)	3.6	3.6	3.6	3.6	3.6
λ_p (-10%)	7.2	7.2	7.2	7.2	7.2
λ_p (5%)	-3.6	-3.6	3.6	3.6	3.6
λ_p (10%)	-7.2	-7.2	7.2	7.2	7.2
θ_p (-5%)	-0.4	0.4	0	0.4	0.3
θ_p (-20%)	-2.6	2.6	0.2	2.6	1.9
θ_p (5%)	-0.3	0.3	0	0.3	0.2
θ_p (12%)	-0.5	0.5	0	0.5	0.3
C (-5%)	-1.5	8.7	0	8.7	4.9
C (-10%)	-0.9	15.3	0.1	15.3	9.0
C (5%)	-9.2	2.1	0.2	9.2	4.0
C (10%)	-17.8	3.6	0.3	17.8	8.1

Note: e_{min} : minimum error; e_{max} : maximum error; $|e|_{min}$: minimum absolute error; $|e|_{max}$: maximum absolute error; nRMSE: nominal RMSE. The part in the bracket is the perturbation. C: The perturbation is add in all of the B_x , B_y , B_z , D , I , λ_p , θ_p . B_x , B_y , B_z at the surface, and D , I are from IGRF model on Oct. 1, 2005 and at the latitude of 40° N.

The second case, on the other hand, is that θ , λ_p and θ_p can be derived from B_x , B_y , B_z (or D , I), eg., through equation (11). This may occur in the paleo-magnetism. Similar to the first case, we add different perturbations to each quantity above as shown in Table

2. The corresponding maximum and minimum error, absolute error, and nominal RMSE, respectively, are also shown in Table 2.

We still take B_x as an example to illustrate. The error curves are shown in Figure 4. It can be seen that Figure 4 is similar to Figure 3, but the maximum error, the minimum error, and the nominal RMSE are less. From Table 2 it is known that these errors are about -5.5° , 0.2° , and 3.7° for the perturbation of -5% , respectively.

From Table 2, it is also found that the errors caused by I is the largest, whose nRMSE is 13.9° even at the perturbation of -5% ; then B_z , then B_x , and the last is D . For D , the nRMSE is less than 2.0° even at the perturbation of $\pm 50\%$. Therefore reasonable longitude inversion demands more accurate I .

Furthermore, in the calculation in the second case, it is found that when we add simultaneously some equal perturbations to B_x, B_y and B_z , the corresponding errors are almost the same to those without adding perturbations. In fact, this is a clear result because such a case is equivalent to equation (10). Therefore the longitudes derived with equation (7) should have smaller errors than those from (9), if the conditions above hold.

4. REFERENCE PALEO-LONGITUDE OF THREE CONTINENTS AND INDO-ASIA COLLISION

In this section, we give two simple applications of the method in the section 2 to the paleo-magnetic data. We firstly estimate the synthetic paleo-longitudes of three continents for the last 200 Ma based on the synthetic data (Schettino and Scotese, 2005). And then we infer the paleo-longitude Indo-Asia collision base on the paleo-magnetic data (Dupont-Nivet et al., 2010).

4.1. Synthetic paleo-longitude of three continents. Schettino and Scotese (2005) presented a new technique to analyse paleo-magnetic data and produced smoothed curves of paleo-latitude, declination and paleo-pole for seven major continents. These curves fit the available paleo-magnetic data. We use directly the curves to estimate the synthetic paleo-longitudes for the continents of North America, Eurasia and India. That is, the regression value of paleo-latitude and declination, synthetic paleopole coordinates for the reference points in these three continents, are adopted here. These references points are: Southwest Hudson Bay (55°N , 270°E) in North America, West Siberian lowlands (60°N , 70°E) in Eurasia, and (24°N , 77°E) in India. It should be noted firstly that synthetic paleo-latitudes here are optimization solutions, so do the synthetic paleo-longitudes; And secondly the errors from the regression value of paleo-latitude and declination, synthetic paleopole coordinates are not taken into account.

Figure 5-7 show the synthetic paleo-positions for North America, Eurasia and India, respectively. In each figure, subfigure a shows the variation of synthetic paleo-longitudes with the geological time; subfigure b the synthetic paleo-latitudes; subfigure c the synthetic paleo-longitude vs. synthetic paleo-latitude; subfigure d the space and time evolution of the corresponding continent. Table 3 shows the synthetic paleo-positions of the reference sites for these three continents from -200 Ma to present at 20-Ma intervals. In the following we illustrate briefly one by one, and omit the word of "synthetic" (eg., synthetic paleo-longitude just referred to as paleo-longitude).

Table 2: Errors caused by B_x , B_y , B_z , etc., when θ , λ_p and θ_p can be derived from B_x , B_y , B_z (or D , I).

Variable (Perturbation)	e_{min} (°E)	e_{max} (°E)	$ e _{min}$ (°E)	$ e _{max}$ (°E)	nRMSE (°E)
B_x, B_y, B_z (0%)	-2.1	2.1	0	2.1	1.4
B_x (-5%)	-5.5	5.4	0.2	5.5	3.7
B_x (-10%)	-12.9	12.9	0.4	12.9	9.1
B_x (5%)	-9.1	9.3	0.3	9.3	6.2
B_x (10%)	-15.5	16.7	0.5	16.7	10.9
B_y (-5%)	-2.0	2.0	0	2.0	1.3
B_y (-50%)	-0.9	0.9	0	0.9	0.4
B_y (5%)	-2.2	2.2	0	2.2	1.5
B_y (50%)	-3.5	3.5	0.2	3.5	2.6
B_z (-5%)	-9.2	9.4	0.3	9.4	6.4
B_z (-10%)	-15.9	17.0	0.6	17.0	11.7
B_z (5%)	-5.6	5.5	0.2	5.6	3.7
B_z (10%)	-13.1	13.1	0.3	13.1	8.7
D (-5%)	-2.2	2.2	0	2.2	1.4
D (-50%)	-3.6	3.9	0	3.9	1.8
D (5%)	-2.1	2.1	0	2.1	1.4
D (50%)	-1.8	1.8	0	1.8	1.2
I (-5%)	-17.9	18.9	0.7	18.9	13.9
I (-10%)	-45.5	45.3	1.2	45.5	30.0
I (5%)	-17.9	17.9	0.3	17.9	11.3
I (10%)	-41.0	41.1	0.4	41.1	25.6
D/I (-5%)	-18.3	19.9	0.7	19.9	14.1
D/I (10%)	-46.8	46.9	1.1	46.9	31.3
D/I (5%)	-17.1	17.0	0.4	17.1	11.0
D/I (10%)	-37.8	37.8	0.5	37.8	24.2

Note: e_{min} : minimum error; e_{max} : maximum error; $|e|_{min}$: minimum absolute error; $|e|_{max}$: maximum absolute error; nRMSE: nominal RMSE. The part in the bracket is the perturbation. D/I : The perturbation is add in both D and I . B_x, B_y, B_z at the surface, and D , I are from IGRF model on Oct. 1, 2005 and at the latitude of 40° N.

North America. Comparing Figure 5a with Figure 5b shows that both paleo-longitudes and paleo-latitudes of the reference point had a similar evolution with geological time like an oblique inversely U-shape. The paleo-longitudes had a change of nearly 90° from -200 Ma to about -100 Ma. After -100 Ma, paleo-longitudes changed a little between -100 Ma and -1.0 Ma. Reflected in Figure 5c, four phases of movement and rotation are clearly distinguishable. During the first phase, the reference point was located in the southwest of the map at -200 Ma, and then it moved to the northeast till -100 Ma. A slight clockwise rotation from -200 Ma to -160 Ma accompanied this northeastward movement, followed by a slight counterclockwise rotation till -100 Ma. In the second phase, the reference point rotated and moved to the southwest again from -100 Ma to -40 Ma. Then it moved westward

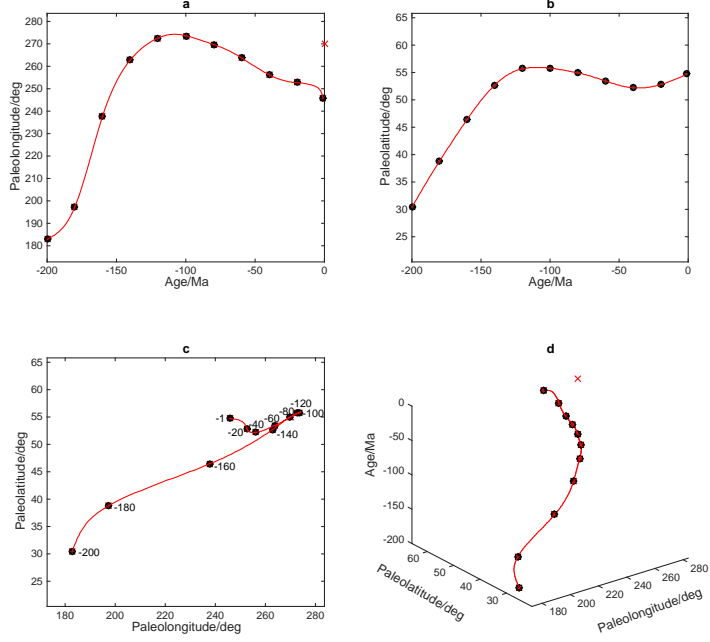


Fig. 5: Synthetic paleo-position of a reference point in North America at (55°N, 270°E) during the last 200 Ma. a. Synthetic paleo-longitudes vs. geological time; b. Synthetic paleo-latitudes vs. geological time (Data is from Schettino and Scotese (2005)); c. Synthetic paleo-latitudes vs. Synthetic paleo-longitudes; d. Synthetic paleo-latitudes and synthetic paleo-longitudes vs. geological time. The red cross is the reference point. (The same to hereinafter.)

till -1.0 Ma during the third phase along a path to an inversely "S", but soon it moved eastward during the last phase to its present position. The paleo-longitude and paleo-latitude had little variation from the second to the fourth phase, indicating the North America is relatively stable during these three phases.

Eurasia. Comparing Figure 6a with Figure 6b shows that paleo-longitudes of the reference point had a nearly antisymmetry evolution with the paleo-latitude from -200 Ma to -20 Ma. The paleo-longitudes had a change of almost 60° from -200 Ma to about -130 Ma. After -120 Ma, paleo-longitudes changed a little between -120 Ma and -20 Ma, then increased by 30°. Reflected in Figure 6c, the trajectory can also be divided into four phases. During the first phase, the reference point was located in the northwest of the map at -200 Ma, and then it moved to the southeast till -130 Ma. A slight counterclockwise rotation accompanied this southeastward movement. In the second phase, the reference point moved northwestward first from -120 Ma to -100 Ma, then southeastward till -60 Ma, finally northwestward again till -20 Ma. During the second phase, the trajectory made a knot. After this, the reference point moved eastward till -1.0 Ma during the third phase, but

Table 3: Synthetic paleo-position for the reference points in North America, Eurasia, and India from -200 Ma to present.

Age(Ma)	North America		Eurasia		India	
	$\lambda(^{\circ}\text{E})$	$\phi(^{\circ}\text{N})$	$\lambda(^{\circ}\text{E})$	$\phi(^{\circ}\text{N})$	$\lambda(^{\circ}\text{E})$	$\phi(^{\circ}\text{N})$
0.0	270.0	55.0	75.0	60.0	77.0	24.0
-1.0	245.7	54.7	123.1	59.4	139.9 (?)	23.0
-20.0	252.7	52.8	90.5	58.9	351.0(? 9.0)	16.5
-40.0	256.3	52.2	92.5	57.7	0.9	4.8
-60.0	263.8	53.5	97.0	56.1	8.6	-13.6
-80.0	269.7	54.9	95.5	56.3	18.0	-30.8
-100.0	273.6	55.8	92.0	57.3	25.7	-39.2
-120.0	272.6	55.7	103.1	55.1	29.1	-42.1
-140.0	262.8	52.7	100.3	54.3	33.0	-39.5
-160.0	237.8	46.5	74.0	60.3	39.2	-34.2
-180.0	197.4	38.8	55.3	68.5	45.2	-29.1
-200.0	182.8	30.4	52.1	72.9	48.1	-25.2

Note: Data for ϕ and Age are all from Schettino and Scotese (2005).

soon it moved westward during the last phase to its present position. The paleo-longitude and paleo-latitude also had little variation from the second to the fourth phase, indicating the Eurasia is also relatively stable during these three phases.

India. Before the illustration, it should be pointed out we modify a paleo-longitude at -20 Ma for the reference point from 351.0°E to 9.0°E (See also in Table 3). Otherwise, India had to move nearly 360° during 20 Ma which may be impossible. And we plot the Figure 7 with the data in Table 3 rather than smooth data like Figure 5-6.

Comparing Figure 7a with Figure 7b shows that both paleo-longitudes and paleo-latitudes of the reference point had a similar evolution with geological time like an oblique U-shape. The paleo-longitudes decreased almost linearly from -200 Ma to about -20 Ma. After -20 Ma, the paleo-longitude increased considerably. Reflected in Figure 7c, four phases of movement and rotation are clearly distinguishable, but on the whole the trajectory was simple. The reference point in India rotated clockwise from -200 Ma to -1.0 Ma. During the first phase, the reference point moved slowly southwestward till -120 Ma, followed by a rotation and moved northwestward till -40 Ma in the second phase. In the third phase, the reference point rotated and moved eastward -40 Ma to 1.0 Ma. Then it moved westward during the last phase to its present position.

Also, we think the paleo-longitude at -1.0 Ma may be problematic because the reference point had to move about 130° in about 20 Ma. We infer it should be located between 9°E and 77°E . This problem is also remarked with a question mark in the Figure 7a, b and d.

4.2. Reference paleo-longitude of Indo-Asia collision. The Indo-Asia continental collision was one of the most profound tectonic events in Cenozoic time. Where and when this event occurred is crucial for continental dynamic models. Scientists of paleo-magnetism

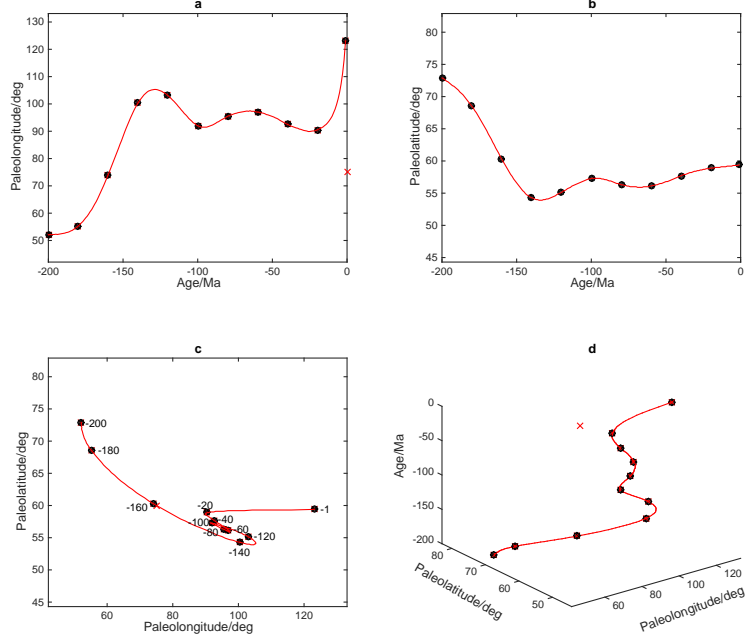


Fig. 6: Synthetic paleo-position of a reference point in Eurasia at (60°N, 70°E) during the last 200 Ma.

thought that the collision range of paleo-latitude was from 5°N to 30°N at 40-60 Ma (eg., Westphal and Pozzi 1983; Chen et al. 1993; Liebke et al. 2010). Based on new data, Dupont-Nivet et al. (2010) suggested that India-Asia collision was at 22.8 ± 4.2 °N and 46 ± 8 Ma. Here we use further their data to estimate the paleo-longitude for this collision. The corresponding results are listed in Table 4.

Table 4: Paleo-poistion for Lhasa terrane and the Tethyan Himalaya

	Age(Ma)	ϕ_s (°N)	λ_s (°E)	ϕ (°N)	λ (°E)	ϕ_p (°N)	λ_p (°E)
L	50.5	30.0	91.1	24.1 ± 4.2	$132.9_{-15.5}^{+27.6}$	81.2	221.4
	87.5	30.0	91.1	22.0 ± 2.5	$54.8_{-8.0}^{+9.7}$	76.7	327.1
	95.0	30.7	91.2	22.7 ± 6.0	$126.3_{-16.5}^{+25.4}$	76.3	213.8
T	59.0	28.3	88.5	6.7 ± 3.1	$6.9_{-1.1}^{+1.5}$	68.2	277.1
	68.0	28.3	88.5	-5.7 ± 3.5	$279.5_{-10.5}^{+26.2}$	55.8	261.6
S	45.7	29.0	88.0	22.8 ± 4.2	$132.6_{-14.7}^{+27.2}$	81.2	221.4

Note: ϕ_s , λ_s : site latitude, site longitude; ϕ , λ : paleo-latitude, paleo-longitude; ϕ_p , λ_p : paleopole latitude, paleopole longitude. L: Lhasa terrane; T: Tethyan Himalaya; S: Suture. All data except λ are from Dupont-Nivet et al. (2010).

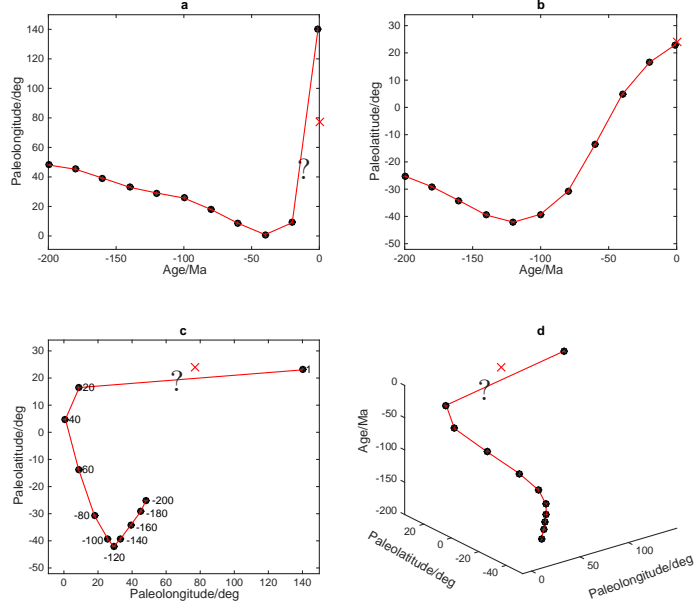


Fig. 7: Synthetic paleo-position of a reference point in India at (24°N, 77°E) during the last 200 Ma.

From Table 4, it can be seen the the paleo-position for India-Asia collision was at $22.8 \pm 4.2^\circ\text{N}$ and $132.6 \pm 14.7^\circ\text{E}$, if this collision occurred at the suture here.

On the other hand, assuming India-Asia collision can be understood as the "intersection" between the trajectory of the Lhasa terrane and Tethyan Himalaya in a (2+1)-dimensional space (2-dimensional space space+1-dimensional time) as shown in Figure 8, rather than that in the usual 2-dimensional space of paleo-latitude vs. geological time, we can get another paleo-position and time of this collision at $12.8 \pm 3.9^\circ\text{N}$ and $101.7 \pm 12^\circ\text{E}$ and $-63.6 \pm 0.6 \pm 5.8 \pm 0.3 \text{ Ma}$ with the data in Table 4. It should be pointed out that this "intersection" is in least squares sense, and this result is only a conjecture that must be constrained or demonstrated by other data.

5. DISCUSSIONS

Here we provide an approach to estimate the paleo-position, especially the paleo-longitude, through paleo-magnetic measurements, as shown in equation (5) in section 2. In theory, we should solve this equation to obtain λ , θ , and K_p simultaneously, through the measurements of B_x , B_y , B_z and the known θ_p , and λ_p . This involves two problems. The first is how to get accurately the θ_p , and λ_p . Except the method we adopted in this paper, constructing the reference poles for a certain geological age may be an alternative good way. This demands a large amount of accurate paleo-magnetic measurements and close

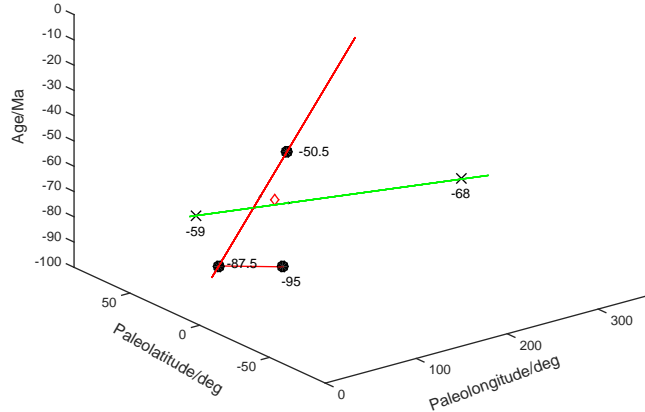


Fig. 8: Paleo-position and time of India-Asia collision. The red line is the trajectory of the Lhasa terrane, green the Tethyan Himalaya. The diamond is the possible position ($12.8^{+3.9}_{-3.6}{}^{\circ}\text{N}$, $101.7^{+12}_{-5.8}{}^{\circ}\text{E}$, $-63.6^{+0.6}_{-0.3}\text{ Ma}$) of the collision.

cooperation of scientists of paleo-magnetism. At present, there is a lot of databases can be used for this purpose, such as IAGA paleo-magnetic databases (McElhinny and Lock, 1996; McElhinny and McFadden, 1997; McElhinny et al., 1998), IAGA paleointensity database (Perrin et al., 1998; Perrin and Schnepp, 2004), Absolute Palaeointensity (PINT) Database (Biggin et al., 2010; Veikkolainen et al., 2017), Magnetics Information Consortium (MagIC) (Jarboe et al., 2012), Precambrian database (PALEOMAGIA) (Veikkolainen et al., 2017), and so on.

The second problem is how to solve the nonlinear equation (5), even if B_x , B_y , B_z are measured and θ_p , and λ_p are known. We have tried many methods, such as homotopy continuation method (Decarolis et al., 2005), artificial neural network inversion tool (Ružek, 2008), a globally optimal iterative algorithm using the best descent vector (Liu and Atluri, 2012), and so on. However, in most cases the results derived are not those we want. Therefore, it is necessary to develop efficient algorithms for solving the nonlinear equation (5), if the first problem is solved.

The approach (equation (7), (9)) used in this paper, which has been shown in section 2, can overcome the difficulties above at a certain extent. If θ (I), λ_p , and θ_p are accurate, the longitude can be derived perfectly. Experiments on synthetic data in the section 3 demonstrate this success. This method demands mainly accurate B_x , B_z , and/or I . When this approach is used in paleo-magnetism as shown in section 2.3 and 4, there is a defect in theory that g_1^1 and h_1^1 are omitted when we estimate θ , θ_p and λ_p by the traditional way (equation (4) and (11)), but they are taken into account in equation (3) and (5). In this

paper we cannot eliminate this defect, and new approaches should be developed. However, as shown in the section (3), if the error in θ (I) can be controlled in a reasonable range, the paleo-longitudes estimated by our approach should be acceptable, especially in the case that B_x (J_x), B_y (J_y) and B_z (J_z) have the same errors.

6. CONCLUSIONS

We associate B_x, B_y, B_z with K_p, θ_p and λ_p through equation (5), in which the strongest component (g_1^0) of the geomagnetic field and the next strongest term (g_1^1, h_1^1) are all taken into account. With this equation, longitude λ can be derived in theory.

Based on equation (5), we obtain two explicit formulae (equation (7) and (9)) to estimate λ through the measured magnetic data for the given θ, θ_p and λ_p . With synthetic data of B_x, B_y, B_z or declination (D) and inclination(I) from IGRF model, we derived the setting longitudes perfectly through these two formulae.

Errors in these two explicit formulae caused by B_x (e_{B_x}) is greater than those by B_z (e_{B_z}), then $e_{B_z} > e_{\lambda_p} > e_I > e_D > e_{B_y} > e_{\theta_p}$ when these quantities are independent and can be obtained or given by other methods; And $e_I > e_{B_z} > e_{B_x} > e_D$ when θ, λ_p and θ_p can be derived from B_x, B_y, B_z (or D, I). Therefore, the errors are mainly from B_x, B_z or I .

For paleo-magnetic data, paleo-longitudes from these two explicit formulae, for example, those in the section 4, could be used as reference, because of the defect in theory when we estimate θ, θ_p and λ_p and the inaccuracy in traditional paleo-magnetic way. To get more accurate results, constraints from other geo-methods are necessary.

References

- Alldredge, L. R., and Hurwitz, L., 1964. Radial dipoles as the sources of the Earth's main magnetic field, *J. Geophys. Res.*, 69 (12), 2631-2640.
- Biggin, A. J., McCormack, A., and Roberts, A., 2010. Paleointensity database updated and upgraded. *EOS Transactions American Geophysical Union* 91, 15.
- Chen, Y., Cogne, J. P., Courtillot, V., Tapponnier, P., and Zhou, X. Y., 1993. Cretaceous paleomagnetic results from western Tibet and tectonic implications, *J. geophys. Res.*, 98, 17981-18000.
- Decarolis F., Mayer R., Santamaria M., 2005. Homotopy continuation method: An algorithm for the fixed point and Newton homotopy methods with some examples, <http://people.bu.edu/fdc/decarolis-research.htm>.

Doubrovine, P. V., Steinberger, B., and Torsvik, T. H., 2012. Absolute plate motions in a reference frame defined by moving hot spots in the Pacific, Atlantic, and Indian oceans, *J. Geophys. Res.*, 117, B09101, doi:10.1029/2011JB009072.

Dupont-Nivet, G., Lippert, P. C., van Hinsbergen, D. J. J., Meijers, M .J .M., and Kapp, P., 2010. Palaeolatitude and age of the Indo-Asia collision: paleomagnetic constraints, *Geophys.J. Int.*, 182, 1189-1198, doi: 10.1111/j.1365-246X.2010.04697.x.

Hurwitz, L., 1960. Eccentric dipoles and spherical harmonic analysis, *J. Geophys. Res.*, 65, 2555-2556.

International Association of Geomagnetism and Aeronomy, Working Group V-MOD, 2010. International Geomagnetic Reference Field: the eleventh generation, *Geophys. J. Int.*, 183(3), 1216-1230,doi:10.1111/j.1365-246X.2010.04804.x.

Jarboe, N. A., Koppers, A. A., Tauxe, L., Minnett, R., and Constable, C., 2012. The online MagIC Database: data archiving, compilation, and visualization for the geomagnetic, paleomagnetic and rock magnetic communities, Abstract GP31A-1063 (American Geophysical Union Fall Meeting, San Francisco, CA.

Kono, M., and Tanaka, H., 1995. Mapping the Gauss coefficients to the pole and the models of paleosecular variation, *J. Geomag. Geoelectr.*, 47, 115-130.

Lanza, R., Meloni, A., 2006. The Earth's magnetism: An introduction for geologists, Springer-Verlag Berlin Heidelberg.

Liebke, U., Appel, E., Neumann, U., Antolin, B., Lin, D., and Qiang, X., 2010. Position of the Lhasa terrane prior to India-Asia collision derived from paleomagnetic inclinations of 53 Ma old dykes of the Linzhou Basin: constraints on the age of collision and post-collisional shortening within the Tibetan Plateau, *Geophys. J. Int.*, 182(3), 1199-1215 doi:10.1111/j.1365-246X.2010.04698.x.

Liu C. S., and Atluri S. N., 2012. A globally optimal iterative algorithm using the best descent vector $\dot{x} = \lambda[\alpha_c F + B^T F]$, with the critical value α_c , for solving a system of nonlinear algebraic equations $F(x) = 0$. *CMES*, 84 (6), 575-601.

Müller, R. D., Royer, J. Y. and Lawver, L. A., 1993. Revised plate motions relative to the hotspots from combined Atlantic and Indian Ocean hotspot tracks, *Geology*, 21(3), 275-278.

McElhinny, M. W. and Lock, J., 1996. IAGA paleomagnetic databases with Access, *Surv. Geophys.*, 17, 575-591.

McElhinny, M. W. and McFadden, P. L., 1997. Palaeosecular variation over the past 5 Myr based on a new generalized database, *Geophys. J. Int.*, 131, 240-252.

McElhinny, M. W., Opdyke, N .D. and Pisarevsky, S. A., 1998. Worldwide database for magnetostratigraphy available, *EOS, Trans. Amer. Geophys. Union*, 79, 167.

Mitchell, R. N., Kilian, T. M., and Evans, D. A., 2012. Supercontinent cycles and the calculation of absolute paleolongitude in deep time, *Nature*, 482(7384), 208-211.

Morgan, W. J., 1971. Convection plumes in the lower mantle, *Nature*, 230, 42C43.

O'Neill, C., Müller, R. D., and Steinberger, B., 2005. On the uncertainties in hot spot reconstructions and the significance of moving hot spot reference frames, *Geochem. Geophys. Geosyst.*, 6, Q04003, doi:10.1029/2004GC000784.

Perrin, M., and Schnepp, E., 2004. IAGA paleointensity database:distribution and quality of the data set. *Phys. Earth. Planet. Int* 147, 255-267.

Perrin, M., Schnepp, E. and Shcherbakov, V., 1998. Update of the paleointensity database, *EOS, Trans. Amer. Geophys. Union*, 79, 198.

Ružek, B., 2008. ANNIT: Artificial Neural Network Inversion Tool. <http://www.ig.cas.cz/en/personal-pages/bohuslav-ruzek/anno/>

Schettino, A., and Scotese, C. R., 2005. Apparent polar wander paths for the major continents (200 Ma to the present day): a paleomagnetic reference frame for global plate tectonic reconstructions, *Geophys. J. Int.*, 163, 727-759, doi:10.1111/j.1365-246X.2005.02638.x.

Torsvik, T. H., Müller, R. D, Van der Voo, R., Steinberger, B., and Gaina C., 2008a. Global plate motion frames: Toward a unified model, *Rev. Geophys.*, 46, RG3004, doi:10.1029/2007RG000227.

Torsvik, T. H., Steinberger, B., Cocks, L. R. M., and Burke, K., 2008b. Longitude: Linking Earths ancient surface to its deep interior, *Earth Planet. Sci. Lett.*, 276(3), 273-282.

Turcotte, D. L., Schubert, G., 2014. *Geodynamics* (3rd ed.). Cambridge University Press.

van der Meer, D. G., Spakman, W., van Hinsbergen, D. J., Amaru, M. L., and Torsvik, T. H., 2010. Towards absolute plate motions constrained by lower-mantle slab remnants, *Nat. Geosci.*, 3(1), 36-40.

Veikkolainen, T. H., Biggin, A. J., Pesonen, L. J., Evans, D. A., and Jarboe, N. A., 2017. Data Descriptor: Advancing Precambrian paleomagnetism with the PALEOMAGIA and PINT(QPI) databases, *Scientific Data*, 4:170068, doi: 10.1038/sdata.2017.68.

Westphal, M., and Pozzi, J. P., 1983. Paleomagnetic and plate tectonic constraints on the movement of Tibet, *Tectonophysics*, 98, 1-10.

Wu, L., and Kravchinsky, V. A., 2014. Derivation of paleolongitude from the geometric parametrization of apparent polar wander path: Implication for absolute plate motion reconstruction, *Geophys. Res. Lett.*, 41, doi:10.1002/2014GL060080.

Wu, L., Kravchinsky, V. A., and Potter, D. K., 2015. PMTec: A new MATLAB toolbox for absolute plate motion reconstructions from paleomagnetism, *Computers & Geosciences*, 82, 139-151.

COLLEGE OF EARTH SCIENCES, UNIVERSITY OF CHINESE ACADEMY OF SCIENCES, BEIJING, PRC, 100049

E-mail address: wrq1973@ucas.ac.cn